Febrile temperature enhances *Plasmodium falciparum* cytoadhesion by disrupting the endothelial glycocalyx

Viola Introini[1 *], Rory Long[1,2], Olawunmi Rashidat Oyerinde[1], Silvia Sanz Sender[1], Frank Stein[3], Gyu Min Hwang[1,4], Borja Lopez Gutierrez[1], Karl Boynton Seydel[5,6,], Gretchen Birbeck[6,7,8], Maria Bernabeu[1*]

[1] European Molecular Biology Laboratory (EMBL) Barcelona, Barcelona, Spain

[2] Heidelberg University, Faculty of Biosciences, Heidelberg, Germany

[3] European Molecular Biology Laboratory (EMBL) Heidelberg, Proteomics Core Facility, Heidelberg, Germany.

[4] Heidelberg, University, Faculty of Engineering Sciences, Heidelberg, Germany

[5] Department of Osteopathic Medical Specialties, College of Osteopathic Medicine, Michigan State University, East Lansing

[6] Blantyre Malaria Project, Kamuzu University of Health Sciences, Blantyre, Malawi

[7] Epilepsy Division, Department of Neurology, University of Rochester, Rochester, New York

[8] University Teaching Hospitals Neurology Research Office, Lusaka, Zambia

*Correspondence

maria.bernabeu@embl.es

viola.introini@embl.es

Abstract

Fever, a universal host defense in infection and inflammation, paradoxically contributes to neurological complications in malaria. While febrile temperatures enhance the expression of parasite virulence proteins that mediate vascular adhesion and disease severity, its effects in the endothelium remain elusive. Here we present a 3D fever-on-a-chip model that recapitulates human brain and lung microvessels under febrile conditions. Short febrile episodes at 40 °C, common in treated cerebral malaria patients, rapidly enhanced iRBC and immune cell binding under flow. Mechanistically, we demonstrated that this phenotype was driven by endothelial glycocalyx shedding, which exposed endothelial receptors EPCR and ICAM-1. Preserving glycocalyx integrity with a broad MMP inhibitor prevented the temperature-induced rise in cytoadhesion. These findings identify fever as a host-specific amplifier of vascular pathology in malaria and highlight endothelial-protective or antipyretic interventions as important strategies to mitigate febrile microvascular pathology.

Main

Fever is an ancient and metabolically costly host response to infection and inflammation, conserved across vertebrates. This tighly regulated process is initated when injury- and pathogen-associated molecular patterns trigger immune response and cellular secretion of prostaglandin E2 (PGE2)[1,2], a lipid effector molecule that activates thermoregulatory neuronal circuits in the hypothalamus to rapidly elevate core body temperature[3]. By transiently raising body temperature, fever restricts microbial fitness, slowing replication, and promoting immune clearance of diverse viral and bacterial pathogens[4]. Yet, it is not universally beneficial for the host, and fever prevention improves outcomes in diseases such as sepsis[5], neurological injury[6], and malaria[7].

Fever is a hallmark of malaria infection and a consistent predictor of severity[8,9]. A detrimental role of fever has been recently exemplified by seizure reduction after aggressive antipyretic treatment[10]. Central to severe malaria pathogenesis is the cytoadherence of *P. falciparum*-infected red blood cells (iRBCs) to the vascular endothelium[11], mediated by clonally variant *P. falciparum* erythrocyte membrane protein 1 (PfEMP1) proteins[12,13] with binding to intercellular adhesion molecule 1 (ICAM-1) and endothelial protein C receptor (EPCR) strongly linked with severe disease[14]. On the parasite side, febrile temperatures profoundly reshape iRBC biology[15] inducing cytoskeletal remodelling[16] and accelerating PfEMP1 surface expression[,17–19], changes that mechanically translate into rapid increase in iRBC stiffness[20], adhesion[21,22], and endothelial contact[19]. At the immune level, fever mobilises host systemic innate and adaptive immune responses,

promoting neutrophil and T cell vascular recruitment[23] and cytokine release[24]. Altogether, these findings position fever as a potent promoter of vascular interaction with both iRBCs and immune cells. Yet studies have focused almost exclusively on pathogen-driven mechanisms, leaving the endothelial response to febrile temperatures poorly understood — a critical gap for host-directed therapeutic strategies.

Here, we employ a bioengineered human fever-on-a-chip microvascular model to dissect how febrile temperatures affect the endothelium and regulate *P. falciparum* iRBC and immune cell adhesion.

Paediatric patients experience high fever despite antipyretic treatment

To characterise febrile dynamics in malaria, we analysed continuous temperature recordings from 146 children enrolled in a randomised controlled trial of aggressive antipyretic treatment for malaria Zambia and Malawi. All participants presented central nervous system symptoms including impaired consciousness and/or seizures, and 72–83% fulfilled the clinical definition of cerebral malaria (CM)[7,10]. Core temperature was measured every 2-4 minutes over 72 hours using a monitoring patch. The present analysis was restricted to children in the control group, who received World Health Organisation (WHO)-recommended treatment with acetaminophen for temperatures over 38.5°C. Despite antipyretic therapy, all patients developed fever, with 25% reaching body temperatures between 39-40 °C, and 10% reaching ≥ 40 °C (**Fig. 1a**). The average fever duration was 1 hour for ≥ 40 °C and 1.7 hours for ≥ 39 °C, with some episodes persisting for several hours (**Fig. 1b**). These findings demonstrate that short episodes of fever are common in CM patients, even under current WHO-recommended fever management.

Febrile temperature increases iRBC binding in 3D brain microvessels

To determine whether hyperthermia influences *P. falciparum* binding to endothelial cells, we employed a bioengineered 3D microvascular model that replicates flow-driven cytoadherence. The platform consists of a microfluidic network of 13x13 channels of 120 µm diameter embedded in a collagen hydrogel, recapitulating a wide range of flow velocities spanning 0.4–15 mm s^{-1} – comparable to those found in the brain arteriovenous microcirculation (0.4–8 mm s^{-1})[25,26] (**Fig. 1c**). The device displays regions exposed to a wall shear stress (WSS) > 1 dyn/cm^2 being representative of physiological flow observed in healthy venules (1–5 dyn/cm^2)[7,17] and WSS < 1 dyn/cm^2 being representative of pathological flow conditions likely found in occluded microvasculature[27,28]. Human brain microvascular endothelial cells (HBMECs) are seeded into the network, and after 3 days in culture, they form fully endothelialised 3D microvessels (**Fig. 1d**). To experimentally model clinical malarial fever episodes, we exposed our engineered 3D human brain microvessel system to 40 °C for 1 hour prior to iRBC perfusion, mimicking the hyperthermic episodes observed in paediatric CM. Since increased temperature affects medium viscosity and density, WSS profiles were simulated at both normothermic (37 °C) and febrile (40 °C) temperatures, showing minimal differences (**Extended Data Fig. 1a**). After incubation of microvessels for 1 hour at either 37 °C or 40 °C,

91 normothermic *P. falciparum*-iRBC were perfused for 30 minutes at the same temperature as the vessel
92 incubation (**Fig. 1e**). Binding was quantified along the outer edges of the microvascular grid, and
93 fluorescent areas containing cytoadhered *P. falciparum*-iRBC were defined as the sequestered area
94 (**Extended Data Fig. 1b**). Multiple clonal lines of *P. falciparum*-iRBCs expressing predominantly single
95 PfEMP1 variants (**Extended Data Fig 2a-b**), including HB3var03 (EPCR-ICAM-1 binder), IT4var19
96 (EPCR binder), and IT4var31 (ICAM-1/CD36 binder), exhibited significantly increased binding at 40 °C
97 across multiple WSS conditions (**Fig. 1f-h**). Temperature did not affect uninfected RBC binding, which
98 remained negligiblele (**Extended Data Fig. 3**). At febrile temperature, ICAM-1 binders (HB3var03 and
99 IT4var31) presented increased binding across all WSS demonstrated, while the EPCR binder (IT4var19)
100 showed increased binding only at higher WSS (>1 dyn/cm²). As a negative control, we used a CSA-binding
101 line expressing var2csa, which mediates placental sequestration. NF54var2csa showed minimal binding at
102 37 °C and no changes at 40 °C, indicating that increased iRBC binding at fever-range temperatures occurred
103 in parasite lines that presented tropism for the brain endothelium (**Fig. 1i**). No significant temperature-
104 dependent changes were observed in endothelial junction organisation, microvessel diameter, endothelial
105 cell area, perimeter, or circularity, except for a slight non-signigicant increase in intracellular von
106 Willebrand Factor (vWF) mean fluorescence intensity (MFI), ruling out major heat-induced vessel
107 remodelling (**Extended Data Fig. 4a-f**). Together, these data show that febrile temperature promotes *P.*
108 *falciparum*-iRBC binding to endothelial cells in a PfEMP1- and flow-dependent manner.

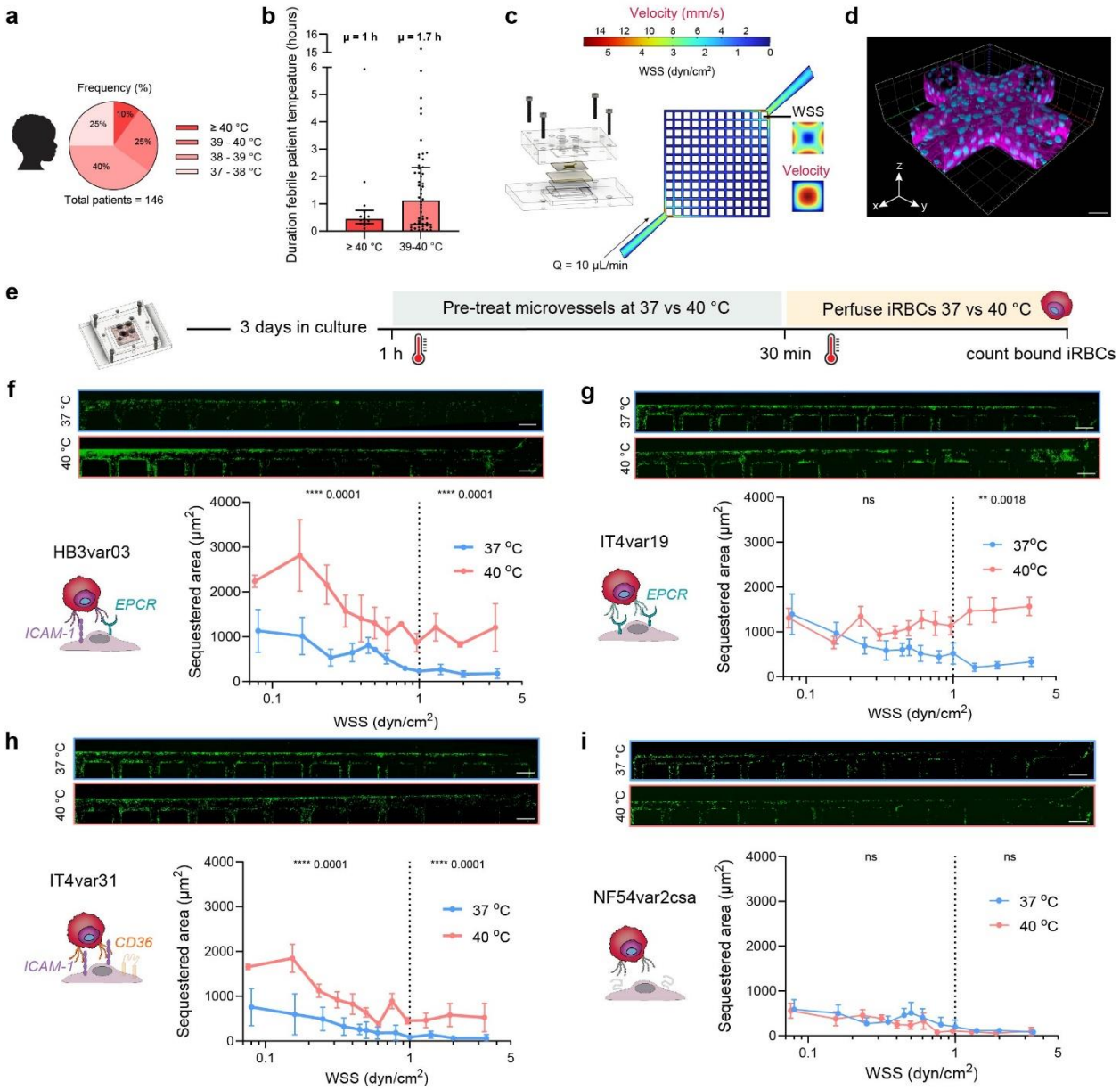

Fig. 1. Fever quantification in paediatric malaria patients and *P. falciparum*-iRBC binding at 37 and 40 °C to 3D microvessels. a, Distribution of maximum body temperature data during admission from 146 paediatric malaria cases in Zambia and Malawi treated with antipyretics as described in Methods. **b,** Duration of high fever episodes ≥ 40 °C or between 39 and 40 °C. Bar plot represent median and interquartile range; μ indicates group mean. **c,** Simulated mid-plane flow velocity in the grid network prior to collagen remodelling by HBMECs (see Methods). Inset: lumen cross-section velocity and WSS at first branch (black line).**d,** Volumetric reconstruction of a microvessel network grid cross section labelled with VE-cadherin antibody (magenta) and nuclear staining by DAPI (blue). Scale bar = 50 μm. **e,** Schematic representation of the binding assay workflow. **f-i,** Receptor binding schematic and iRBC sequestered areas at 37 °C and 40 °C across WSS for: f, HB3var03; g, IT4var19; h, IT4var31; i, NF54var2csa. Medians are represented by dots and interquartile range by error bars. Statistical analysis of binned regions (< 1 dyn/cm^2 and ≥ 1 dyn/cm^2) (dotted line) was determined by Mann-Whitney U test (n = 6 independent biological replicates for HB3var03, IT4var19, and IT4var31; n = 4 for NF54var2csa). Scale bars = 200 μm.

123 **EPCR and ICAM-1 mediate temperature-driven iRBC and neutrophil binding without changes in**
124 **receptor expression**

125 To investigate whether endothelial receptors are responsible for the mechanism underlying increased
126 sequestration at 40 ºC, we inhibited *P. falciparum*-iRBC binding using anti-ICAM-1 and anti-EPCR
127 antibodies. Systematic inhibition of ICAM-1, EPCR, or both at 40 ºC significantly reduced binding of both
128 *P. falciparum* lines HB3var03 and IT4var19 compared to an IgG control. Cytoadhesion at 37 and 40 °C did
129 not present any statistical difference after antibody treatment, reaching a baseline residual non-specific
130 binding, specially under pathological low flow (WSS < 1 dyn/cm²) (**Fig. 2a,b, Extended Data Fig. 5a-d**).
131 To examine the broader implications of febrile temperature-induced changes in vascular adhesion, we
132 perfused neutrophils into microvessels pre-incubated at either 37 °C or 40 ºC, known to bind to the
133 endothelium in an ICAM-1-mediated manner. Indeed, exposure to 40 ºC significantly increased
134 cytoadhesion of neutrophils at pathological low flow but not at higher WSS (**Fig. 2c**).
135 To determine whether a temperature-induced increase in expression of ICAM-1 or EPCR contributed to the
136 increase binding of *P. falciparum*-iRBC and neutrophils, we assessed total endothelial proteins by
137 employing quantitative mass spectrometry using tandem mass tag (TMT) labelling. Whole-proteome
138 analysis of HBMEC monolayers exposed to 40 °C for 1 hour revealed minimal changes in protein
139 expression (**Figure 2d**), with only a handful of significantly upregulated proteins (e.g., SFSWAP, UQCC1,
140 DPP9) and one downregulated transcript (SNRPD3). These proteins are primarily associated with RNA
141 splicing, mitochondrial function, or inflammasome regulation, while protein levels of EPCR and ICAM-1
142 remained unchanged. Although 1h exposure is probably insufficient for substantial changes at the protein
143 level, further analysis revealed slight increases in heparanase (HSPE), heat shock proteins (HSPs), and
144 prostaglandin synthesis pathway enzimes (PTGs), suggesting early fever-mediated endothelial stress and
145 initiation of heparan sulfate shedding (**Extended Data Fig.6**). We next used flow cytometry to quantify
146 both the surface levels and the proportion of cells expressing ICAM-1 and EPCR after heat (**Figure 2e,**
147 **Extended Data Fig. 7**). No differences were observed for ICAM-1 and EPCR, and CD36, which is
148 minimally expressed in the brain, while CD31 present at 40 °C confirms endothelial cell viability at febrile
149 temperature (**Figure 2e, Extended Data Fig. 7**). Altogether, *P. falciparum*-iRBC binding at 40 ºC is
150 mediated by ICAM-1 and EPCR, however such increase is not explained by differences in the receptor
151 surface expression.
152

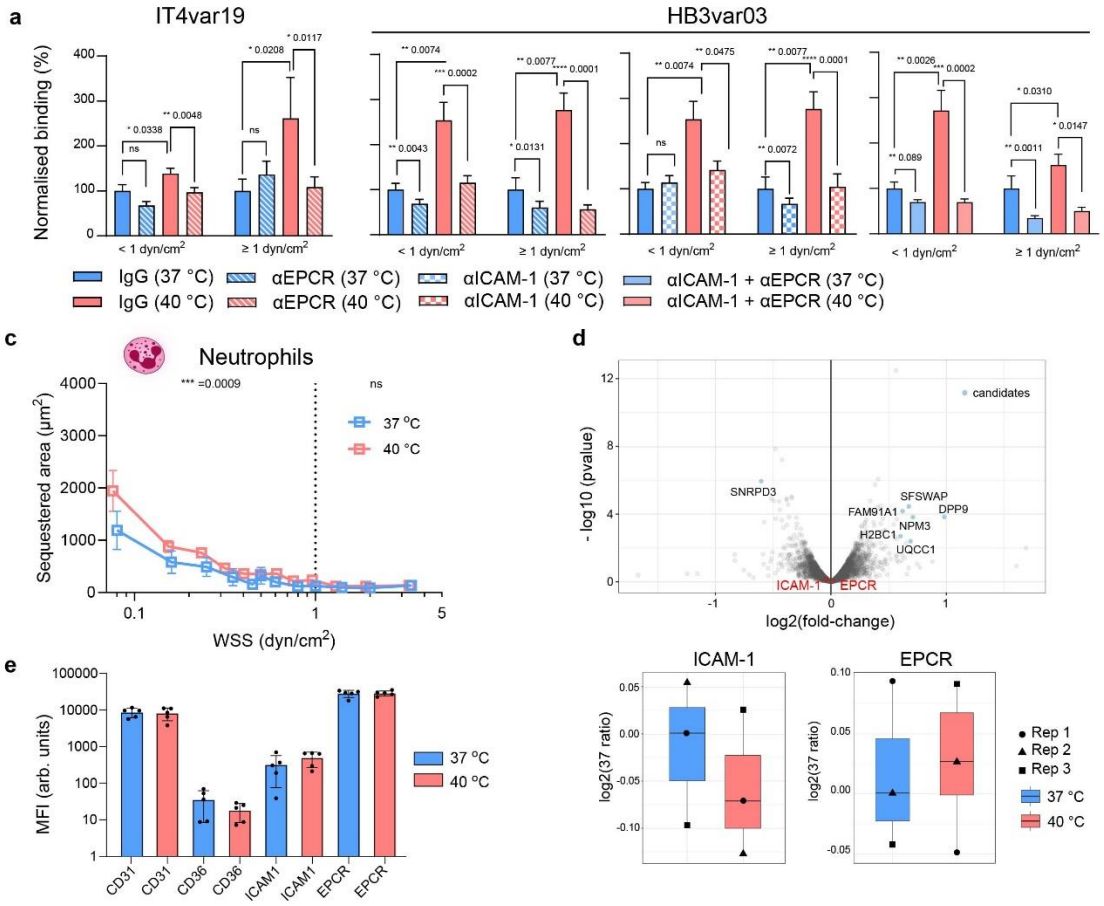

Fig. 2. Receptor-mediated binding of *P. falciparum* and neutrophils at febrile temperature occurs without altering endothelial protein level. a, Binding of IT4var19 strain iRBCs at 37 °C or 40 °C in the presence of IgG isotype control (filled) or anti-EPCR mAb 252 antibody (stripes). **b**, Binding of HB3var03 strain iRBCs at 37 °C or 40 °C in the presence of IgG isotype control (filled) or both anti-EPCR mAb 252 (stripes), anti-ICAM-1 mAb 15.2 (squares), and both (light colour). Percentage of binding for each treatment is normalised to the respective IgG control at 37 °C. Bars represent mean ± SEM. Statistical analysis for the two WSS regions WSS <1 dyn/cm² and WSS ≥ 1 dyn/cm² using Mann-Whitney U test; n= 4-6 independent microvessels. Stratified data can be found in Extended Fig. 5. **c,** Sequestered neutrophil area at 37 °C and 40 °C across WSS (medians as lines and interquartile ranges as error bars). Statistical analysis for the two WSS regions WSS <1 dyn/cm² and WSS ≥ 1 dyn/cm² using Mann-Whitney U test; n = 4 biological replicates per condition. **d,** Volcano plot of differential protein expression of HBMEC monolayer exposed to 37 °C or 40 °C for 1 h (top), with labeled candidates showing statistically significant changes in protein expression. ICAM1 and EPCR differential protein expression (bottom). *n* = 3 independent biological replicates. **e**, MFI of HBMEC surface level expression by flow cytometry after 1h at 37 °C and 40 °C. Bars represent mean ± standard deviation (SD) (n = 5-6 biological replicates).

Febrile temperature promotes endothelial glycocalyx shedding

The glycocalyx is a carbohydrate-rich layer that limits endothelial receptor accessibility[29,30]. To test whether febrile temperature disrupts the endothelial glycocalyx, we exposed HBMECs to 40 °C. Staining revealed

175 a marked loss of sialic acids (**Fig. 3a**), heparan sulfate (**Fig. 3b**), and syndecan-4 (**Fig. 3c**). Syndecan-4, the
176 most abundant proteoglycan, also showed significant shedding (**Fig. 3d**). The decrease in glycocalyx
177 molecules was comparable to that induced by neuraminidase (NA) treatment, which cleaves terminal sialic
178 acid residues from membrane glycoproteins[31]. To determine if temperature-induced glycocalyx shedding
179 occurs in the vasculature of other organs, we fabricated microvessels from primary human pulmonary artery
180 endothelial cells (HPAECs), an important site of iRBC cytoadhesion[32,33]. Following 40 °C incubation, lung
181 microvessels displayed increased shedding of syndecan-1 (**Fig. 3e**), a marker of lung vasculature pathology
182 in malaria[34,35] and other microbial infections[36]. This was accompanied by a decrease in sialic acid but not
183 of heparan sulfate, similar to NA treatment (**Fig. 3f, g, Extended Data Fig. 8a, b**).
184 To determine whether glycocalyx degradation is responsible for enhanced *P. falciparum*-iRBC binding, we
185 pretreated 3D brain microvessels with NA for 30 minutes at 37 °C, followed by perfusion with HB3var03
186 and IT4var19 *P. falciparum*-iRBCs. Binding doubled at WSS < 1 dyn/cm² for both lines, reaching levels
187 similar to those observed at 40 °C (**Fig. 4h, i**). However, NA treatment failed to reproduce increased binding
188 observed at WSS ≥ 1 dyn/cm², specially for the EPCR binder, IT4var19 (**Fig. 4i**). Incubation with anti-
189 EPCR and ICAM-1 inhibitory antibodies in combination with NA treatment, brought *P. falciparum*-iRBC
190 binding levels back to baseline, thus confirming enhanced PfEMP1-receptor interactions upon glycocalyx
191 disruption (**Extended Data Fig. 9a, b**). These findings support a model in which breakdown of sialic acids
192 and other glycan structures by fever-induced temperatures act as co-factors that facilitate PfEMP1-mediated
193 adhesion predominantly under low WSS.

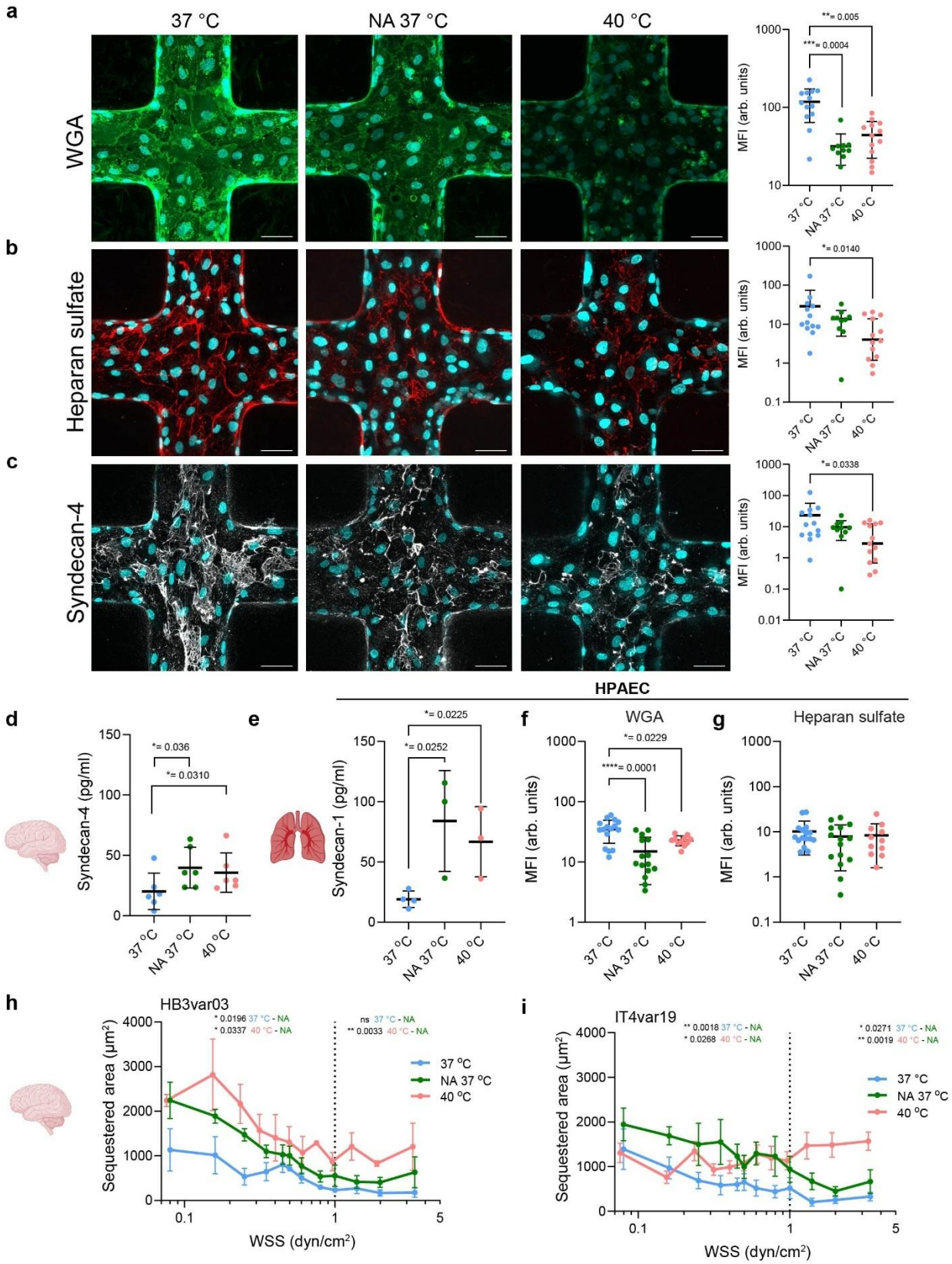
a
37 °C
NA 37 °C
40 °C
WGA
MFI (arb. units)
**= 0.005
***= 0.0004
b
Heparan sulfate
*= 0.0140
c
Syndecan-4
*= 0.0338
HPAEC
d
Syndecan-4 (pg/ml)
*= 0.036
*= 0.0310
e
Syndecan-1 (pg/ml)
*= 0.0225
*= 0.0252
f
WGA
MFI (arb. units)
*= 0.0229
****= 0.0001
g
Heparan sulfate
h
HB3var03
Sequestered area (µm²)
WSS (dyn/cm²)
* 0.0196 37 °C - NA
* 0.0337 40 °C - NA
ns 37 °C - NA
** 0.0033 40 °C - NA
37 °C
NA 37 °C
40 °C
i
IT4var19
** 0.0018 37 °C - NA
* 0.0268 40 °C - NA
* 0.0271 37 °C - NA
** 0.0019 40 °C - NA

194

Fig. 3. Febrile temperature induces shedding of the endothelial glycocalyx. Immunofluorescence z-stack of microvessel cross sections (left) and MFI normalised by number of cells quantified by DAPI (left) of **a**, sialic acids labelled with FITC-conjugated Wheat Germ Agglutinin (WGA), **b,** heparan sulfate and **c**, syndecan-4; box plots show mean ± SD, n = 4 microvessels per condition, each dots is a region of interest. Scale bars: 50 µm. **d,** Syndecan-4 shedding quantified by ELISA of 3D brain microvessel supernatants following exposure to 37 °C or 40 °C. **e**, Syndecan-1 shedding quantified by ELISA of 3D pulmonary microvessel supernatants. Graphs show mean ± SD, which each dot is from a different microvessel batch. Immunofluorescence MFI quantification of **f**, sialic acids labelled with WGA, and **g**, heparan sulfate in 3D pulmonary microvessels; box plots show mean ± SD, n = 4 microvessels per condition, each dots is a region of interest. Conditions in **a-g** include 37 °C or 40 °C incubation for 1 hour, and NA treatment for 30 min at 37 °C (1 U/mL). Statistical analysis was done by one-way ANOVA with Tukey's multiple comparisons or pairwise comparisons were performed using the two-sided Mann-Whitney U test. **h-i)** HB3var03 and IT4var19 binding to 3D brain microvessels treated with NA (n = 5 microvessels) compared to 37 °C and 40 °C (n = 6 microvessels). Medians are shown as dots; error bars represent interquartile range. Statistical analysis by Kruskal-Wallis test for binned WSS regions (< 1 dyn/cm² vs ≥ 1 dyn/cm²; dotted line).

Matrix metalloproteinase inhibition preserves the glycocalyx and reverses temperature-induced cytoadhesion

To investigate the mechanisms driving glycocalyx degradation at febrile temperature, we analysed the secretion of angiogenic mediators, inflammatory cytokines, proteolytic enzymes, and endothelial markers from HBMEC monolayers using a semi-quantitative protein array. After 1 hour at 40 °C, HBMEC exhibited significantly increased secretion of extracellular matrix remodelling proteases, such as matrix metalloproteinase-1 (MMP-1) and vascular inflammatory markers including angiopoietin-2 (ANGPT2). No significant increases in pro-inflammatory cytokines IL-6, IL-1 β, and TNF-α, were observed after 1 hour at 40 °C (**Fig. 4a**). As MMP-1 has been shown to be linked to glycocalyx degradation[37], we next examined whether the broad MMP inhibitor batimastat reverses enhanced iRBC cytoadhesion. Indeed, binding of both HB3var03 and IT4var19 *P. falciparum*-iRBCs at 40 °C was significantly reduced by microvessel batimastat pre-treatment at both healthy and pathological WSS, with sequestration levels comparable to those at 37 °C (**Fig. 4b, c**). Furthermore, we confirmed that batimastat stabilised the glycocalyx, preventing sialic acid, heparan sulfate, and syndecan-4 removal at 40 °C (**Fig. 4d-f**). Altogether, our results show that short-term exposure of endothelial cells to febrile temperatures promotes iRBC binding by MMP-mediated glycocalyx breakdown, and suggests that protection of the glycocalyx could be a potential therapeutic avenue in the prevention of iRBC cytoadhesion during severe malaria.

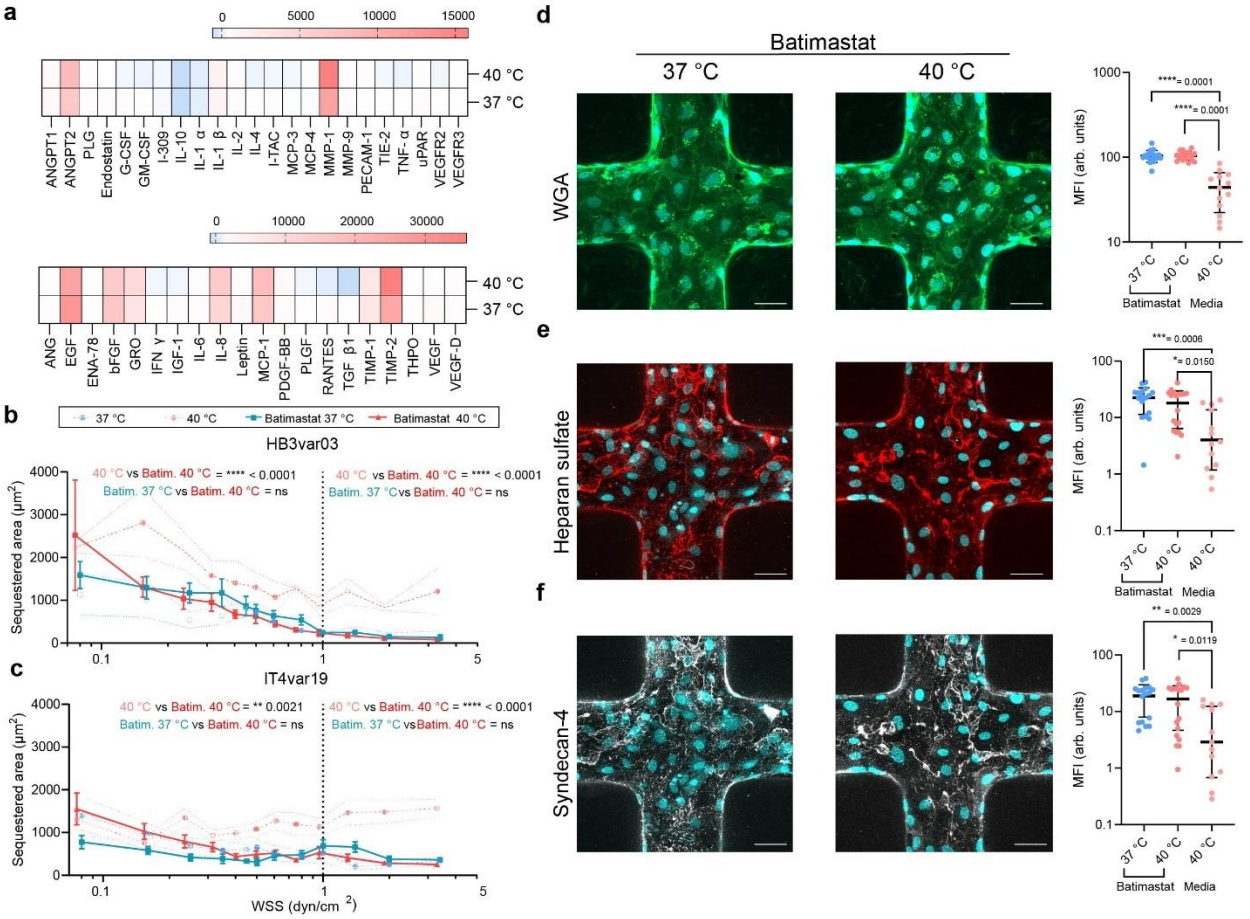

Fig. 4. Analysis of MMP1 secretion, *P. falciparum*-iRBC binding and endothelial glycocalyx protection after treatment with the MMP inhibitor, batimastat a, Quantification of angiogenesis-related molecule secretion from HBMEC monolayers after 1 h at 37 °C or 40 °C. Supernatants pooled from n=3 biological replicates and normalised as described in Methods. **b-c,** HB3var03 and IT4var19 binding after exposure of batimastat-pre-treated microvessels to 37 °C or 40 °C (n = 4 brain microvessels). Median ± error bars representing interquartile range. Statistical analysis by Kruskal-Wallis test for binned WSS regions (< 1 dyn/cm² vs ≥ 1 dyn/cm²; dotted line). **d-f,** Z-projection immunofluorescence images of batimastat pre-treated microvessel junctions exposed to 37 °C or 40 °C and labelled for WGA, heparan sulfate, syndecan-4 and DAPI (cyab) (left) and measured glycocalyx marker MFI normalised by number of cells using DAPI (right) (n = 4 brain microvessels, dots represent quanfied ROI). Statistical analysis by one-way ANOVA with Tukey's multiple comparisons; box plots show mean ± SD. Scale bars = 50 μm.

Discussion

Although fever generally exerts protective effects for the host against infection, our findings reveal that during severe malaria infection it may paradoxically amplify pathology by promoting cytoadhesion of *Plasmodium falciparum*–iRBCs. This study shows that brief exposure to high febrile temperatures causes glycocalyx shedding, increasing interactions with blood cells, including *Plasmodium falciparum*-iRBC and neutrophil cytoadhesion. Enhanced cytoadhesion has important clinical implications as elevated

sequestered parasite biomass in the microvasculature is a key component of severe malaria[38,39,14]. Increased adhesion during fever could directly worsen disease progression, by promoting vascular obstruction and blood-brain barrier disruption through inflammatory and permeability-inducing pathways[40–43], as netosis or neutrophil extravasation are linked to CM[44,45] and acute respiratory distress syndrome[46], respectively. This aligns with clinical observations linking higher febrile episodes to adverse outcomes, including epilepsy, long-term disabilities and cognitive impairments[47].

A key finding of this study is that febrile temperature promotes degradation of the endothelial glycocalyx. The glycocalyx is a dynamic network of sugars and proteins lining the vascular endothelium, which forms a barrier that limits direct interaction of endothelial cells with circulating blood cells and vascular components. Its breakdown is common in severe *P. falciparum*[48–51], *vivax*, and *knowlesi* malaria[35], with fever emerging as a unifying symptom across malaria infections, despite the three parasites presenting significant differences in biology. Recovery of the glycocalyx is slow, requiring about 20 hours after enzymatic degradation *in vitro*[52] and up to 7 days *in vivo*[53]. The glycocalyx varies in thickness from 0.2 to 4.5 μm[54], being more prominent in the brain than in the lung[55,56]. Major cytoadhesion receptors, such as the ~18.7 nm[57,58] ICAM-1 and the even smaller EPCR, lie well beneath this layer. Our results show that short episodes of fever degrade the brain and lung endothelial glycocalyx, exposing these normally shielded receptors and thereby facilitating *P. falciparum*-iRBC and neutrophil binding under flow[29]. We confirmed this by the enzymatic removal of terminal sialic acids with neuraminidase, which reproduced the febrile binding phenotype under pathological flow conditions (WSS < 1 dyn/cm²) for both HB3var03 and IT4var19. Neuraminidase mostly affects the outermost negative-charged glycocalyx layer. By contrast, febrile-range temperatures induced shedding of deeper components, such as syndecan-4 and heparan sulfate. This mechanistic distinction could explain why neuraminidase treatment alone failed to replicate the full febrile binding profile at higher, physiological WSS (≥ 1 dyn/cm²), in which *P. falciparum*-iRBCs are only exposed briefly to the endothelial surface.

Our study also shed light on the mechanism of temperature-dependent glycocalyx shedding. Although 1 hour incubation at 40 °C did not elicit a detectable increase in pro-inflammatory cytokines such as IL-6, IL-1 β, IFN γ or TNF-α, or enhanced EPCR and ICAM-1 expression, hyperthermia triggered a rapid release of MMP-1 and Angiopoietin-2, both implicated in glycocalyx breakdown[59] and CM pathology[60,61,62]. Both molecules are stored in intracellular endothelial vesicles and can rapidly be released[63], contributing to extracellular matrix remodelling and directly facilitating glycocalyx degradation[64]. Previous findings suggest that temperature-induced MMP1 release could be further amplified by *P. falciparum*, as endothelial cells upregulate MMP1–3 in response to iRBCs at elevated temperatures[65]. Additionally, expression of heparanase, an endoglycosidase that cleaves heparan sulfate and plays a role in neutrophil adhesion during

sepsis[55], was increased following exposure to febrile temperatures. As MMPs can synergise with heparanase to enhance its expression, this may provide an additional mechanism for temperature-dependent glycocalyx breakdown[66]. Importantly, we demonstrated that the MMP inhibitor batimastat can prevent glycocalyx shedding[67] and the temperature-dependent increase in binding to EPCR and ICAM-1, suggesting potential therapeutic benefit, in agreement with previous mouse experimental cerebral malaria studies showing delayed mortality[68]. However, batimastat's broad-spectrum activity, lack of specificity and off-target effects limit its clinical development and suggest the use of more specific MMP inhibitors[69]. In the absence of effective host-directed therapies for severe malaria, our findings underscore the need for aggressive antipyretic treatment.

Beyond malaria, hyperthermia profoundly shapes vascular and immune interactions. It accelerates neutrophil migration[70] and extracellular trap formation[71], enhances leukocyte adhesion[37,72–75], and promotes MMP release in sepsis[76] and stroke[77], driving basement membrane breakdown. Glycocalyx dysregulation is increasingly recognised as a central determinant of vascular vulnerability, implicated in viral lung injury[30,78], sepsis[55], ageing and neurodegeneration[79]. Consistently, hyperthermia worsens outcomes in stroke[9] and hypoxic–ischemic brain injury[80] by disrupting the blood–brain barrier and causing brain edema[81] —paralleling CM pathology. Our findings therefore extend to a broader principle: febrile temperature destabilises the glycocalyx and amplifies microvascular pathology across infectious and inflammatory diseases.

Our flow-based microvessel chip overcomes the restrictions of traditional assays used to study the effects on febrile temperatures on *P. falciparum*-iRBC interactions, that relied on recombinant proteins, which lack glycans or protein ability to freely move and rearrange on the plasma membrane. For example, discrepancies have been found when using force-spectroscopy to measure binding strength to recombinant proteins, showing a weaker binding to recombinant receptors[18,82] after heating, while binding studies with iRBCs maintained increased cytoadhesion to cell lines[18]. The 3D platform has been previously validated in studies of *P. falciparum* interactions with EPCR and ICAM-1[83], and in testing inhibitory effect of plasma[84] or monoclonal antibodies[85]. An advantage of our system, is that it allows to decouple the temperature-effect of fever, independently of elevated pro-inflammatory cytokine levels, key pyrogens that upregulates endothelial receptors, such as ICAM-1. The independent tuning of physical and biological parameters also represents and advantage over hyperthermia animal models. A limitation is that it remains plausable that rapid mechanical modifications at the surface of the *P. falciparum*-iRBC could further contribute to increased cytoadhesion. However, the strong inhibition of binding with batimastat suggests that glycocalyx disruption is a major responsible for increase binding. Future studies should examine the impact of glycocalyx impairment on bond dynamics under flow, the combined effect of hyperthermia and

inflammatory signalling in malaria, and extend the model with additional blood–brain barrier cell types or immune cells to directly assess febrile contributions CM pathology.

Methods

Body temperature measurements in patients

Body temperature data were collected from 146 children (ages 2–11) who received the WHO recommended treatment with 15 mg/kg acetaminophen every 6 hours as needed for temperatures ≥ 38.5 °C. Participants were enrolled at Queen Elizabeth Central Hospital (Blantyre, Malawi), University Teaching Hospitals Children's Hospital (Lusaka, Zambia), and Chipata Central Hospital (Chipata, Zambia)[7,10]. All had *P. falciparum* infection confirmed by blood smear or rapid diagnostic test and presented with central nervous system symptoms (impaired consciousness and/or seizures) of whom 72–83% met CM criteria. Temperatures were recorded via a body patch every 2–4 minutes over a 72-hour period, during which most children defervesce. Ethics approvals: Biomedical Research Ethics Committee (Zambia): 003-06-18, University of Rochester Research Subjects Review Board: 00067717, and College of Medicine Research and Ethics Committee (Malawi): P.10/17/2298.

Plasmodium falciparum culture

P. falciparum clones HB3 and IT4 were cultured and selected for expression of PfEMP1 variants HB3VAR03, IT4VAR19, and IT4var31 in human O+ erythrocytes in RPMI-1640 medium (Gibco) containing 25 mM HEPES, 1.5 g/L gentamicin, 0.4 mM hypoxanthine, 26.8 mM sodium bicarbonate, 5 mM glucose, and 10% human type AB+ serum (complete RMPI). Parasites were grown in a gas mixture of 90% N2, 5% CO2, and 5% O2 and parasitemia was regularly checked by Giemsa staining. Cultures were regularly panned and monitored for correct PfEMP1 expression on primary human brain microvascular endothelial cells (HBMECs). *P. falciparum* parasites were synchronized weekly using 5% sorbitol to select for ring-stage parasites.

3D brain microvessel fabrication

Primary HBMECs (Cell Systems ACBRI 376) and primary human pulmonary artery endothelial cells (HPAECs) (Lonza CC-2530) were grown in a flask coated with poly-L-lysine (Sigma #P8920) up to passage 9 before they were seeded in microvessels. 3D microvessel devices were prepared as described previously[83]. The top part of the microvessels is generated by injecting type I collagen (7.5 mg/mL) into the space created between the top plexiglass jig and a polydimethylsiloxane (PDMS) mold with a 13-by-13 grid geometry, fabricated using soft lithography. The bottom part consists of a flat layer of collagen, compressed between

343 a flat PDMS stamp and a 22-by-22 mm coverslip positioned on the bottom jig. After 30 minutes of gelation
344 at 37 °C, the PDMS stamps were removed, and the top and bottom jigs were sealed creating a three-
345 dimensional network within the collagen hydrogel. Primary HBMECs or HPAECs were seeded at a
346 concentration of $7x10^6$ cells/mL under gravity-driven flow by adding 8 µL volume increments to the device
347 inlet until reaching full coverage in the microfluidic network. Microvessels were then cultured for up to 3
348 days and fed every 12 hours by gravity-driven flow before performing *P. falciparum* binding experiments.

349 *Temperature-dependent parasite binding assay in 3D brain microvessels*

350 *P. falciparum* cultures were enriched for mature-stage iRBCs using a MACS cell separator with LD columns
351 (Miltenyi Biotec 130-042-901) and diluted to 5×10^6/mL in complete RPMI. The iRBCs were labeled with
352 the membrane dye PKH26 Red Fluorescent Cell Linker Midi Kit (Sigma MIDI26-1KT) according to
353 manufacturer's instructions. For neutrophil binding experiments, neutrophils were isolated from whole
354 blood samples, obtained from the Catalan Blood and Tissue Bank, using the EasySep Direct Human
355 Neutrophil Isolation kit (StemCell 19666) according to manufacturer's instructions. Isolated neutrophils
356 were labeled with the membrane dye PKH26 and resuspended to a concentration of $2.0x10^6$ neutrophils/mL
357 in RPMI 1640 (Sigma) supplemented with 5% heat-inactivated fetal bovine serum (Gibco), 0.1% vascular
358 endothelial growth factor (Lonza), 0.4% recombinant human FGF (Lonza), 0.1% ascorbic acid (Lonza),
359 0.1% R3-insulin-like growth factor (Lonza), 0. 1% recombinant human endothelial growth factor (Lonza),
360 0.5% penicillin/streptomycin (Gibco) and 1% Glutamax (Gibco). The 3D brain microvessels were pre-
361 incubated for 1 hour at either 37 °C or 40 °C. before normothermic iRBCs or neutrophils were perfused for
362 30 min at 37 °C or 40 °C, respectively, at a flow rate of 10 µl/min using a syringe infusion pump (KD
363 Scientific KDS220). After perfusion, a 5-minute wash with EGM-2MV endothelial medium followed at the
364 same flow rate. Microvessels were fixed in 4% PFA for 20 minutes followed by two 10-minute washes in
365 PBS, and stained with DAPI (8 µg/mL). Each 3D microvessel device was used once for each experimental
366 condition. For iRBC binding inhibition experiments with blocking antibodies, microvessels were pretreated
367 for 20 min at the respective temperature before perfusing iRBCs by gravity-driven flow with mouse anti-
368 human ICAM-1 monoclonal antibody (mAb) 15.2 (Abcam; ab20 [5 µg/ml]), rat anti-human EPCR mAb
369 252 (Sigma-Aldrich; E6280-200UL [50 µg/ml]), or mouse (Abcam; ab19443) or rat (Thermo Fisher; 14-
370 4301-85) IgG isotype control. For drug inhibition experiments, microvessels were pretreated with the MMP
371 inhibitor batimastat (R&D systems; 2961) at 5µM for 2-h prior to the 1-h incubation at 37 °C or 40 °C.

372 *Numerical simulation of wall shear stress rates*

373 The flow characteristics of 3D brain microvessels were simulated using COMSOL Multiphysics software,
374 as previously described[83]. Flow in the microvessel network (diameter 120 µm) was assumed to be laminar,
375 and the stationary solver for laminar flow was used with predefined Navier-Stokes equations. Due to the

low hematocrit (<0.1%) used during perfusion, flow was assumed to be Newtonian, and wall shear stress (WSS) rates were calculated based on fluid viscosity of water or culture medium at 37 °C (viscosity of 6.922×10^{-4} Pa s and density of 993.3 kg/m^3) and 40 °C (viscosity of 6.539×10^{-4} Pa s and density of 992.2 kg/m^3). The inlet boundary conditions were defined for the perfusion flow rate of 10 µl/min, and the outlet boundary conditions were set at zero pressure.

Parasite and neutrophil binding quantification

For each device, the edges of the 13-by-13 grid were imaged. A Zeiss LSM 980 AiryScan2 microscope with 10× NA 0.3 objective was used to image cytoadhered iRBCs or neutrophils labeled with PKH26 membrane dye (laser 555 nm) and DAPI-stained parasite and HBMEC nuclei (405 nm laser). DAPI staining was used as control to confirm that HBMEC coverage of the microvessels was uniform. Images were acquired at a 3-µm Z-step size, and projection images of the bottom of the vessel were produced from Z-stacks using Fiji (ImageJ v1.52b) software. The cytoadhered area indicates the area occupied by attached iRBCs across the 12 predefined regions along the edges of the device, as described previously[85]. To minimize flow artifacts, parasite binding was assessed exclusively in the central region of the channel, where flow remains laminar and fully developed, avoiding junctions between branches. Entry and exit regions were excluded, as flow is not fully developed in these regions. Each edge was considered a technical replicate for each device, while each device was considered an independent biological replicate. For statistical analysis, WSS range was divided into 2 regions named pathological[27,28] (<1 dyn/cm²) and physiological (≥1 dyn/cm²)[83,86], in line with flow values observed in postcapillary venules under healthy versus inflammatory conditions.

Immunofluorescence microscopy of 3D microvessels

Fixed 3D brain microvessels were incubated in Background Buster (Innovex #NB306) for 30 minutes and blocking buffer (2% bovine serum albumin, 0.1% Triton X-100 in PBS) for 1 hour. Blocked microvessels were stained overnight at 4 °C with mouse anti-VE-cadherin primary antibody (Abcam, ab33168) and sheep anti-vWF (Bio-Rad, AHP062) at 1:100 dilution. For Glycocalyx staining, microvessels were blocked with 2% bovine serum albumin in PBS for l hour and stained overnight at 4 °C with 1:50 Human anti-Syndecan-4 antibody (R&D Systems, AF2918-S) and 1:100 anti-Heparan Sulfate (Amsbiom, 370255-S). Microvessels were washed six times for 10 minutes with PBS and incubated for 1 hour at RT with 1:250 Alexa-Fluor 488-, Alexa-Fluor 594- or Alexa-Fluor 647-conjugated secondary antibodies (Invitrogen), containing DAPI 2 µg/mL (ThermoFisher, D21490; 1:250). Following secondary antibody incubation, glycocalyx-stained microvessels were labeled with FITC-conjugated Wheat Germ Agglutinin WGA (VWR 29022-1/ 29022-1; 1:50) for 20 minutes at RT. Microvessels were then washed six times for 10 minutes with PBS and imaging was done using a Zeiss LSM 980 AiryScan 2 confocal microscope with a 20× NA

0.8 objective using a 1-µm Z-step. The 3D rendering of a microvessel cross-section shown in **Figure 2** was obtained using Zeiss ZEN v3.3 and Arivis Vision4D v3.5.1 software.

Human Cytokine Antibody Array

For cytokine analysis, supernatants were collected from 2D HBMEC monolayers from n = 3 biological replicates. A human angiogenesis array (Abcam, ab193655) was performed according to the manufacturer's instructions. The relative expression of cytokines (measured by chemiluminescence intensity) was compared between samples exposed to 37 °C and 40 °C for 1 hour, corrected to the negative controls on each array, and normalised to the positive controls as suggested by the kit manufacturer. The blots were visualised and imaged (1 min exposure) using the Fusion FX Spectra (Vilber, France).

ELISA assay

Quantification of Syndecan-4 and Syndecan-1 was performed using the Human Syndecan-4 DuoSet ELISA kit (R&D Systems, DY2918) and Human Syndecan-1 DuoSet ELISA kit (R&D Systems, DY2780), according to manufacturer's instructions. Media from the outlet reservoir of each device was collected after incubation for 1 hour at 37 °C and 40 °C from N = 3-6 experiments at day 3.

Proteomics

<u>Sample Preparation:</u> HBMEC cells were cultured on flasks for three to four days until confluent, and then incubated for 1 h either at 37 °C or 40 °C (total of 3 biological replicates per condition). Cells were lysed in cold RIPA buffer with 1× protease inhibitors, incubated on ice for 15 min, sonicated (5 pulses of 5 min at 0/0.5 high, 5°C), and centrifuged at ~14,000 × g for 15 min. Protein concentration was determined using the BCA assay by incubating 20 µL of samples with 200 µL of BCA working reagent (50:1, Reagent A:B) at 37°C for 30 min, followed by absorbance measurement at 562 nm. Samples were subjected to the SP3 protocol[87,88] on a King Fisher Apex Platform (Thermo Fisher) and peptides were eluted by tryptic digestion (sequencing grade trypsin, Promega) for 5 h at 37°C. Peptides were labelled with TMT6plex[89] Isobaric Label Reagent (ThermoFisher) according the manufacturer's instructions. In short, 0.8 mg reagent was dissolved in 42 µL acetonitrile (100%) and 4 µL of stock was added and incubated for 1h room temperature. Followed by quenching the reaction with 5% hydroxylamine for 15 min at RT. Samples were combined and for further sample clean up an OASIS® HLB µElution Plate (Waters) was used. The TMT6-labelled proteome was fractionated by high-pH reversed-phase carried out on an Agilent 1200 Infinity high-performance liquid chromatography system, equipped with a Gemini C18 column (3 µm, 110 Å, 100 x 1.0 mm, Phenomenex). 48 fractions were collected along with the LC separation that were subsequently pooled into 12 fractions. Pooled fractions were dried under vacuum centrifugation and reconstituted in 10 µL 1% formic acid, 4% acetonitrile and then stored at -80 °C until LC-MS analysis.

440 Data acquisition. Samples were measured on an Q Exactive™ Mass Spectrometer (Thermo) coupled to an
441 UltiMate 3000 RSLC nano LC system (Dionex). Sample was concentrated on a C18 µ-Precolumn (Acclaim
442 PepMap 100, 5µm, 300 µm i.d. x 5 mm, 100 Å) and resolved on a nanoEase™ M/Z HSS T3 column from
443 Waters (75 µm x 250 mm C18, 1.8 µm, 100 Å). Trapping was carried out at a constant flowrate of 30
444 µL/min 0.5% trifluoroacetic acid in water for 4 min. Subsequently, peptides were eluted via the analytical
445 column (solvent A: 0.1% formic acid in water, 3% DMSO) with a constant flow of 0.3 µL/min, with
446 increasing percentage of solvent B (0.1% formic acid in acetonitrile, 3% DMSO) from 2% to 8% in 6 min,
447 8% to 28% in 37 min, from 28% to 40% in 9 min, followed by an increase of B from 40-80% for 3 min and
448 a re-equilibration back to 2% B for 5 min. The peptides were introduced into the mass spectrometer via a
449 Pico-Tip Emitter 360 µm OD x 20 µm ID; 10 µm tip (New Objective) and an applied spray voltage of 2.4
450 kV. The capillary temperature was at 275°C. Settings for the Q Exactive were: Full mass scan (MS1) was
451 acquired with mass range 375-1200 m/z, profile mode, in the orbitrap, resolution of 70000, fill time 10 ms.
452 AGC target 3E6. Data dependent acquisition (DDA) was performed with the resolution of the Orbitrap set
453 to 17500, fill time 50 ms, AGC target of 9E1 ions. Normalized collision energy of 32, HCD, fixed first mass
454 110 m/z.

455 Database search. Fragpipe v21.1 with MSFragger v4.0[90] was used to process the acquired data, which was
456 searched against the homo sapiens Uniprot proteome database (UP000005640, ID9606, 20594 entries,
457 release October 2022) with common contaminants and reversed sequences included. The following
458 modifications were considered as fixed modification: Carbamidomethyl (C) and TMT6 (K). As variable
459 modifications: Acetyl (Protein N-term), Oxidation (M) and TMT6 (N-term). For the MS1 and MS2 scans a
460 mass error tolerance of 20 ppm was set. Further parameters were: Trypsin as protease with an allowance of
461 maximum two missed cleavages; Minimum peptide length of seven amino acids; The false discovery rate
462 on peptide and protein level was set to 0.01.

463 Data analysis. The raw output files of FragPipe (protein.tsv files) were processed using the R programming
464 environment (ISBN 3-900051-07-0). Initial data processing included filtering out contaminants and reverse
465 proteins. Only proteins quantified with at least 2 razor peptides (with Razor.Peptides >= 2) were considered
466 for further analysis. 4203 proteins passed the quality control filters. In order to correct for technical
467 variability, batch effects were removed using the 'removeBatchEffect' function of the limma package on the
468 log2 transformed raw TMT reporter ion intensities ('channel' columns)[91]. Subsequently, normalization was
469 performed using the 'normalizeVSN' function of the limma package (VSN - variance stabilization
470 normalization[92]). Differential expression analysis was performed using the moderated t-test provided by the
471 limma package[91]. The model accounted for replicate information by including it as a factor in the design
472 matrix passed to the 'lmFit' function. Proteins were annotated as hits if they had a false discovery rate (FDR)

below 0.05 and an absolute fold change greater than 2. Proteins were considered candidates if they had an FDR below 0.2 and an absolute fold change greater than 1.5.

Flow cytometry

HBMECs were cultured in flasks for 3–4 days until confluent, then transferred to 6-well plates and incubated for 1 h at either 37 °C or 40 °C. Cells were rinsed with HBSS and detached using 15 mM EDTA in HBSS. A total of 1×10^5 cells were seeded into wells of a 96-well plate and washed once with PBS containing 0.5% BSA at room temperature. Antibody staining was performed on ice, with each step incubated for 30 minutes. The following antibodies were used: goat anti-human EPCR (5 µg/ml; R&D Systems, AF2245), followed by donkey anti-goat Alexa Fluor 647-conjugated secondary antibody (1:400; Invitrogen, A32849); PE-conjugated anti-human ICAM-1 (2 µl per 10^6 cells; Miltenyi Biotec, REA266, 130-120-711) and relative isotype control PE-conjugated human IgG1 (Miltenyi, 130-113-471); FITC-conjugated anti-human CD31 (5 µl per 10^5 cells; BD Pharmingen, 560984) and relative FITC-labelled mouse IgG1 (Abcam, ab18447); FITC-labelled anti-human CD36 (10 µl per 10^5 cells; Abcam, ab39022) and relative FITC-conjugated mouse IgG1 isotype control (2 µg/ml; Abcam, ab106163). Phosphatidylserine (PS)-exposing apoptotic cells were identified using Annexin V mouse anti-human (10 µg/ml; CoraLite 647, Proteintech, 1E6A8) in Annexin V Binding Buffer. All experiments were performed on live cells, and dead cells were excluded using DAPI (ThermoFisher, D21490; 1:600 dilution). The percentage of positive gated cells and mean fluorescence intensity (MFI) were quantified. Data were analysed using FlowJo v10 software (Tree Star Inc.).

Statistical analysis

GraphPad Prism (version 10.2.0) was used for statistical analysis. For normally distributed samples, pairwise comparisons were analysed by unpaired t-test with Welch's correction, while for non-normally distributed samples using Mann-Whitney U test. To compare multiple conditions of normally or non-normally distributed samples we used Kruskal-Wallis test with Dunn's multiple comparisons test and one-way ANOVA with Tukey's multiple comparisons, respectively. P values < 0.05 were considered statistically significant. Values are reported as median (Interquartile Interval), mean ± standard deviation or standard deviation of the mean when indicated. Statistical significance is reported as: $*p < 0.05$, $**p < 0.01$, $***p < 0.001$, $****p < 0.0001$. Parasite binding conditions with low variability were tested in four independent 3D microvessel devices, while conditions with high variability were tested in 6 independent devices.

Data availability

504 The mass spectrometry proteomics data have been deposited to the ProteomeXchange Consortium via the
505 PRIDE [1] partner repository with the dataset identifier PXD063878.
506

507 Acknowledgements

508 The authors thank Jennifer Schwarz and the Proteomics Core Facility at EMBL Heidelberg, the
509 CRG-UPF Flow cytometry facility and Moritz Treeck for sharing the NF54DiCre parasite line.
510 The great majority of this work was funded by the European Research Council (ERC) under the
511 European Union's Horizon 2020 research and innovation program (Grant agreement no. 948088),
512 the EMBL core program funding and contributions from the EMBL Infection Biology Transversal
513 Theme (Transition to Independence Grant to VI). VI was supported by a Marie Skłodowska-Curie
514 Actions post-doctoral fellowship FEBRIS [101026717]), and ORO by the EIPOD-LinC fellowship
515 program, funded by EMBL Marie Skłodowska Curie Actions. FS was supported by the Proteomics
516 Core Facility at EMBL Heidelberg. Patient FEVER study was carried out by GLB and KBS and
517 supported by the NIH grants R01NS102176 and R35NS122265.

518 Authorship contributions

519 Conceptualization: VI, MB; Methodology & validation: VI, RL, MB; Data collection: VI, RL,
520 ORO, SSS, GMH, BLG, KBS, GLB; Formal analysis: VI, FS; Visualization: VI; Writing original
521 draft: VI, RL, MB; Resources: VI, MB; Supervision: MB; Project Administration: VI, MB;
522 Funding Acquisition: VI, MB; All authors gave final approval for publication.

523 Competing interests

524 The authors declare no competing interests.

525

526 # References

527 1. Yamagata, K. *et al.* Coexpression of Microsomal-Type Prostaglandin E Synthase with
528 Cyclooxygenase-2 in Brain Endothelial Cells of Rats during Endotoxin-Induced Fever. *J*
529 *Neurosci* **21**, 2669–2677 (2001).
530 2. Eskilsson, A. *et al.* Immune-Induced Fever Is Dependent on Local But Not Generalized
531 Prostaglandin E2 Synthesis in the Brain. *J. Neurosci.* **37**, 5035–5044 (2017).
532 3. Lazarus, M. *et al.* EP3 prostaglandin receptors in the median preoptic nucleus are critical for
533 fever responses. *Nat Neurosci* **10**, 1131–1133 (2007).
534 4. Evans, S. S., Repasky, E. A. & Fisher, D. T. Fever and the thermal regulation of immunity: the
535 immune system feels the heat. *Nat Rev Immunol* **15**, 335–349 (2015).
536 5. Launey, Y., Nesseler, N., Mallédant, Y. & Seguin, P. Clinical review: fever in septic ICU
537 patients--friend or foe? *Crit Care* **15**, 222 (2011).
538 6. Polderman, K. H. Induced hypothermia and fever control for prevention and treatment of
539 neurological injuries. *Lancet* **371**, 1955–1969 (2008).
540 7. Chilombe, M. B. *et al.* Aggressive antipyretics in central nervous system malaria: Study
541 protocol of a randomized-controlled trial assessing antipyretic efficacy and parasite
542 clearance effects (Malaria FEVER study). *PLOS ONE* **17**, e0268414 (2022).
543 8. Suz, P., Vavilala, M. S., Souter, M., Muangman, S. & Lam, A. M. Clinical Features of Fever
544 Associated With Poor Outcome in Severe Pediatric Traumatic Brain Injury. *Journal of*
545 *Neurosurgical Anesthesiology* **18**, 5 (2006).
546 9. Greer, D. M., Funk, S. E., Reaven, N. L., Ouzounelli, M. & Uman, G. C. Impact of Fever on
547 Outcome in Patients With Stroke and Neurologic Injury. *Stroke* **39**, 3029–3035 (2008).

548 10. Birbeck, G. L. *et al.* Acetaminophen and Ibuprofen in Pediatric Central Nervous System
549 Malaria: A Randomized Clinical Trial. *JAMA Neurology* **81**, 857–865 (2024).
550 11. Miller, L. H., Baruch, D. I., Marsh, K. & Doumbo, O. K. The pathogenic basis of malaria.
551 *Nature* **415**, 673–679 (2002).
552 12. Smith, J. D. *et al.* Switches in Expression of Plasmodium falciparum var Genes Correlate with
553 Changes in Antigenic and Cytoadherent Phenotypes of Infected Erythrocytes. *Cell* **82**, 101–
554 110 (1995).
555 13. Su, X. Z. *et al.* The large diverse gene family var encodes proteins involved in cytoadherence
556 and antigenic variation of Plasmodium falciparum-infected erythrocytes. *Cell* **82**, 89–100
557 (1995).
558 14. Sahu, P. K. *et al.* Determinants of brain swelling in pediatric and adult cerebral malaria. *JCI*
559 *Insight* **6**, e145823 (2021).
560 15. Jones, D. *et al.* Physiological febrile heat stress increases cytoadhesion through increased
561 protein trafficking of Plasmodium falciparum surface proteins into the red blood cell. *eLife*
562 **14**, (2025).
563 16. Oakley, M. S. M. *et al.* Molecular Factors and Biochemical Pathways Induced by Febrile
564 Temperature in Intraerythrocytic *Plasmodium falciparum* Parasites. *Infect Immun* **75**, 2012–
565 2025 (2007).
566 17. Udomsangpetch, R. *et al.* Febrile temperatures induce cytoadherence of ring-stage
567 *Plasmodium falciparum* -infected erythrocytes. *Proc. Natl. Acad. Sci. U.S.A.* **99**, 11825–
568 11829 (2002).

569 18. Carvalho, P. A., Diez-Silva, M., Chen, H., Dao, M. & Suresh, S. Cytoadherence of erythrocytes
570 invaded by Plasmodium falciparum: Quantitative contact-probing of a human malaria
571 receptor. *Acta Biomaterialia* **9**, 6349–6359 (2013).
572 19. Zhang, R., Chandramohanadas, R., Lim, C. T. & Dao, M. Febrile Temperature Elevates the
573 Expression of Phosphatidylserine on Plasmodium falciparum (FCR3CSA) Infected Red Blood
574 Cell Surface Leading to Increased Cytoadhesion. *Sci Rep* **8**, 15022 (2018).
575 20. Marinkovic, M. *et al.* Febrile temperature leads to significant stiffening of *Plasmodium*
576 *falciparum* parasitized erythrocytes. *American Journal of Physiology-Cell Physiology* **296**,
577 C59–C64 (2009).
578 21. Lubiana, P. *et al.* Adhesion between P. falciparum infected erythrocytes and human
579 endothelial receptors follows alternative binding dynamics under flow and febrile
580 conditions. *Sci Rep* **10**, 4548 (2020).
581 22. Dörpinghaus, M. *et al.* Stringent Selection of Knobby Plasmodium falciparum-Infected
582 Erythrocytes during Cytoadhesion at Febrile Temperature. *Microorganisms* **8**, 174 (2020).
583 23. Tulapurkar, M. E. *et al.* Febrile-Range Hyperthermia Modifies Endothelial and Neutrophilic
584 Functions to Promote Extravasation. *Am J Respir Cell Mol Biol* **46**, 807–814 (2012).
585 24. Keitelman, I. A. *et al.* Short-Term Fever-Range Hyperthermia Accelerates NETosis and
586 Reduces Pro-inflammatory Cytokine Secretion by Human Neutrophils. *Front. Immunol.* **10**,
587 (2019).
588 25. Koutsiaris, A. G. *et al.* Volume flow and wall shear stress quantification in the human
589 conjunctival capillaries and post-capillary venules in vivo. *Biorheology* **44**, 375–386 (2007).

590 26. Itoh, Y. & Suzuki, N. Control of brain capillary blood flow. *J Cereb Blood Flow Metab* **32**,
591 1167–1176 (2012).
592 27. Kaul, D. K., Roth, E. J., Nagel, R. L., Howard, R. J. & Handunnetti, S. M. Rosetting of in
593 *Plasmodium falciparum*-infected red blood cells with uninfected red blood cells enhances
594 microvascular obstruction under flow conditions. *Blood* **78**, 812–819 (1991).
595 28. Sahu, P. K. *et al.* Pathogenesis of cerebral malaria: new diagnostic tools, biomarkers, and
596 therapeutic approaches. *Front Cell Infect Microbiol* **5**, 75 (2015).
597 29. Hempel, C., Wang, C. W., Kurtzhals, J. A. & Staalsø, T. Binding of *Plasmodium falciparum* to
598 CD36 can be shielded by the glycocalyx. *Malar J* **16**, 193 (2017).
599 30. Targosz-Korecka, M. *et al.* Endothelial glycocalyx shields the interaction of SARS-CoV-2 spike
600 protein with ACE2 receptors. *Sci Rep* **11**, 12157 (2021).
601 31. Introini, V., Carciati, A., Tomaiuolo, G., Cicuta, P. & Guido, S. Endothelial glycocalyx regulates
602 cytoadherence in *Plasmodium falciparum* malaria. *J. R. Soc. Interface* **15**, 20180773 (2018).
603 32. Corbett, C. E., Duarte, M. I., Lancellotti, C. L., Silva, M. A. & Andrade Júnior, H. F.
604 Cytoadherence in human falciparum malaria as a cause of respiratory distress. *J Trop Med*
605 *Hyg* **92**, 112–120 (1989).
606 33. Van den Steen, P. E. *et al.* Pathogenesis of malaria-associated acute respiratory distress
607 syndrome. *Trends in Parasitology* **29**, 346–358 (2013).
608 34. Bush, M. A. *et al.* Degradation of endothelial glycocalyx in Tanzanian children with
609 Falciparum malaria. *FASEB J* **35**, e21805 (2021).
610 35. Barber, B. E. *et al.* Endothelial glycocalyx degradation and disease severity in Plasmodium
611 vivax and Plasmodium knowlesi malaria. *Sci Rep* **11**, 9741 (2021).

612 36. Park, P. W., Pier, G. B., Hinkes, M. T. & Bernfield, M. Exploitation of syndecan-1 shedding by
613 Pseudomonas aeruginosa enhances virulence. *Nature* **411**, 98–102 (2001).
614 37. Mulivor, A. W. & Lipowsky, H. H. Inhibition of Glycan Shedding and Leukocyte-Endothelial
615 Adhesion in Postcapillary Venules by Suppression of Matrixmetalloprotease Activity with
616 Doxycycline. *Microcirculation* **16**, 657–666 (2009).
617 38. Bernabeu, M. *et al.* Severe adult malaria is associated with specific PfEMP1 adhesion types
618 and high parasite biomass. *Proc Natl Acad Sci U S A* **113**, E3270-3279 (2016).
619 39. Kessler, A. *et al.* Linking EPCR-Binding PfEMP1 to Brain Swelling in Pediatric Cerebral
620 Malaria. *Cell Host Microbe* **22**, 601-614.e5 (2017).
621 40. Gillrie, M. R. *et al.* Src-family kinase–dependent disruption of endothelial barrier function by
622 Plasmodium falciparum merozoite proteins. *Blood* **110**, 3426–3435 (2007).
623 41. Gallego-Delgado, J. *et al.* Angiotensin receptors and β-catenin regulate brain endothelial
624 integrity in malaria. *J Clin Invest* **126**, 4016–4029 (2016).
625 42. Howard, C., Joof, F., Hu, R., Smith, J. D. & Zheng, Y. Probing cerebral malaria inflammation in
626 3D human brain microvessels. *Cell Rep* **42**, 113253 (2023).
627 43. Piatti, L. *et al.* Plasmodium falciparum egress disrupts endothelial junctions and activates
628 JAK-STAT signaling in a microvascular 3D blood-brain barrier model. *Nat Commun* **16**, 7262
629 (2025).
630 44. Knackstedt, S. L. *et al.* Neutrophil extracellular traps drive inflammatory pathogenesis in
631 malaria. *Sci Immunol* **4**, eaaw0336 (2019).
632 45. Du, X. *et al.* PRL2 regulates neutrophil extracellular trap formation which contributes to
633 severe malaria and acute lung injury. *Nat Commun* **15**, 881 (2024).

634 46. Yang, S.-C., Tsai, Y.-F., Pan, Y.-L. & Hwang, T.-L. Understanding the role of neutrophils in acute
635 respiratory distress syndrome. *Biomed J* **44**, 439–446 (2021).
636 47. Birbeck, G. L. *et al.* Blantyre Malaria Project Epilepsy Study (BMPES) of neurological
637 outcomes in retinopathy-positive paediatric cerebral malaria survivors: a prospective cohort
638 study. *The Lancet Neurology* **9**, 1173–1181 (2010).
639 48. Yeo, T. W. *et al.* Glycocalyx breakdown is associated with severe disease and fatal outcome in
640 *Plasmodium falciparum* malaria. *Clin Infect Dis* **69**, 1712–1720 (2019).
641 49. Yeo, T. W. *et al.* Glycocalyx breakdown is increased in African children with cerebral and
642 uncomplicated falciparum malaria. *The FASEB Journal* **33**, 14185–14193 (2019).
643 50. Georgiadou, A. & Cunnington, A. J. Shedding of the vascular endothelial glycocalyx: a
644 common pathway to severe malaria? *Clin Infect Dis* **69**, 1721–1723 (2019).
645 51. Lyimo, E. *et al.* In Vivo Imaging of the Buccal Mucosa Shows Loss of the Endothelial
646 Glycocalyx and Perivascular Hemorrhages in Pediatric Plasmodium falciparum Malaria.
647 *Infect Immun* **88**, e00679-19 (2020).
648 52. Giantsos-Adams, K. M. *et al.* Heparan Sulfate Regrowth Profiles Under Laminar Shear Flow
649 Following Enzymatic Degradation. *Cell Mol Bioeng* **6**, 160–174 (2013).
650 53. Potter, D. R., Jiang, J. & Damiano, E. R. The recovery time course of the endothelial-cell
651 glycocalyx in vivo and its implications in vitro. *Circ Res* **104**, 1318–1325 (2009).
652 54. Reitsma, S., Slaaf, D. W., Vink, H., van Zandvoort, M. A. M. J. & oude Egbrink, M. G. A. The
653 endothelial glycocalyx: composition, functions, and visualization. *Pflugers Arch* **454**, 345–
654 359 (2007).

655 55. Schmidt, E. P. *et al.* The pulmonary endothelial glycocalyx regulates neutrophil adhesion and
656 lung injury during experimental sepsis. *Nat Med* **18**, 1217–1223 (2012).
657 56. Ando, Y. *et al.* Brain-Specific Ultrastructure of Capillary Endothelial Glycocalyx and Its
658 Possible Contribution for Blood Brain Barrier. *Sci Rep* **8**, 17523 (2018).
659 57. Kirchhausen, T., Staunton, D. E. & Springert, T. A. Location of the domains of ICAM-1 by
660 immunolabeling and single-molecule electron microscopy. *Journal of Leukocyte Biology* **53**,
661 342–346 (1993).
662 58. Jun, C.-D. *et al.* Ultrastructure and Function of Dimeric, Soluble Intercellular Adhesion
663 Molecule-1 (ICAM-1)*. *Journal of Biological Chemistry* **276**, 29019–29027 (2001).
664 59. Lukasz, A. *et al.* Endothelial glycocalyx breakdown is mediated by angiopoietin-2.
665 *Cardiovascular Research* **113**, 671–680 (2017).
666 60. Deininger, M. H., Winkler, S., Kremsner, P. G., Meyermann, R. & Schluesener, H. J. Angiogenic
667 proteins in brains of patients who died with cerebral malaria. *Journal of Neuroimmunology*
668 **142**, 101–111 (2003).
669 61. Jain, V. *et al.* Plasma levels of angiopoietin-1 and -2 predict cerebral malaria outcome in
670 Central India. *Malaria Journal* **10**, 383 (2011).
671 62. Conroy, A. L. *et al.* Angiopoietin-2 levels are associated with retinopathy and predict
672 mortality in Malawian children with cerebral malaria: A retrospective case–control study*.
673 *Critical Care Medicine* **40**, 952 (2012).
674 63. Taraboletti, G. *et al.* Shedding of the Matrix Metalloproteinases MMP-2, MMP-9, and MT1-
675 MMP as Membrane Vesicle-Associated Components by Endothelial Cells. *The American*
676 *Journal of Pathology* **160**, 673–680 (2002).

677 64. Endo, K. *et al.* Cleavage of syndecan-1 by membrane type matrix metalloproteinase-1
678 stimulates cell migration. *J Biol Chem* **278**, 40764–40770 (2003).
679 65. Allweier, J. *et al.* Cytoadhesion of Plasmodium falciparum-Infected Red Blood Cells Changes
680 the Expression of Cytokine-, Histone- and Antiviral Protein-Encoding Genes in Brain
681 Endothelial Cells. *Mol Microbiol* **122**, 948–967 (2024).
682 66. Fitzgerald, M., Hayward, I. P., Thomas, A. C., Campbell, G. R. & Campbell, J. H. Matrix
683 metalloproteinase can facilitate the heparanase-induced promotion of phenotype change in
684 vascular smooth muscle cells. *Atherosclerosis* **145**, 97–106 (1999).
685 67. Ramnath, R. D. *et al.* Blocking matrix metalloproteinase-mediated syndecan-4 shedding
686 restores the endothelial glycocalyx and glomerular filtration barrier function in early
687 diabetic kidney disease. *Kidney Int* **97**, 951–965 (2020).
688 68. Hempel, C., Sporring, J. & Kurtzhals, J. A. L. Experimental cerebral malaria is associated with
689 profound loss of both glycan and protein components of the endothelial glycocalyx. *The*
690 *FASEB Journal* **33**, 2058–2071 (2019).
691 69. Dove, A. MMP inhibitors: Glimmers of hope amidst clinical failures. *Nature Medicine* **8**, 95–
692 95 (2002).
693 70. Khachaturyan, G. *et al.* Temperature-sensitive migration dynamics in neutrophil-
694 differentiated HL-60 cells. *Sci Rep* **12**, 7053 (2022).
695 71. Janko, J. *et al.* Neutrophil extracellular traps formation and clearance is enhanced in fever
696 and attenuated in hypothermia. *Front. Immunol.* **14**, (2023).
697 72. Lefor, A. T. *et al.* Hyperthermia increases intercellular adhesion molecule-1 expression and
698 lymphocyte adhesion to endothelial cells. *Surgery* **116**, 214–220; discussion 220-221 (1994).

699 73. Chen, Q. *et al.* Thermal Facilitation of Lymphocyte Trafficking Involves Temporal Induction of
700 Intravascular ICAM-1. *Microcirculation* **16**, 143–158 (2009).
701 74. Chen, Q. *et al.* Fever-range thermal stress promotes lymphocyte trafficking across high
702 endothelial venules via an interleukin 6 trans-signaling mechanism. *Nat Immunol* **7**, 1299–
703 1308 (2006).
704 75. Shah, A. *et al.* Cytokine and adhesion molecule expression in primary human endothelial
705 cells stimulated with fever-range hyperthermia. *Int J Hyperthermia* **18**, 534–551 (2002).
706 76. Yazdan-Ashoori, P. *et al.* Elevated plasma matrix metalloproteinases and their tissue
707 inhibitors in patients with severe sepsis. *J Crit Care* **26**, 556–565 (2011).
708 77. Alam, M., Mohammad, A., Rahman, S., Todd, K. & Shuaib, A. Hyperthermia up-regulates
709 matrix metalloproteinases and accelerates basement membrane degradation in
710 experimental stroke. *Neuroscience Letters* **495**, 135–139 (2011).
711 78. Taghavi, S. *et al.* Glycocalyx degradation and the endotheliopathy of viral infection. *PLOS*
712 *ONE* **17**, e0276232 (2022).
713 79. Shi, S. M. *et al.* Glycocalyx dysregulation impairs blood–brain barrier in ageing and disease.
714 *Nature* **639**, 985–994 (2025).
715 80. Laptook, A. R. & Corbett, R. J. T. The effects of temperature on hypoxic-ischemic brain injury.
716 *Clinics in Perinatology* **29**, 623–649 (2002).
717 81. Kiyatkin, E. A. & Sharma, H. S. Permeability of the blood–brain barrier depends on brain
718 temperature. *Neuroscience* **161**, 926–939 (2009).
719 82. Lim, Y. B. *et al.* Temperature-Induced Catch-Slip to Slip Bond Transit in *Plasmodium*
720 *falciparum*-Infected Erythrocytes. *Biophysical Journal* **118**, 105–116 (2020).

721 83. Bernabeu, M. *et al.* Binding Heterogeneity of Plasmodium falciparum to Engineered 3D
722 Brain Microvessels Is Mediated by EPCR and ICAM-1. *mBio* **10**, e00420-19 (2019).
723 84. Joof, F. *et al.* Plasma From Older Children in Malawi Inhibits Plasmodium falciparum Binding
724 in 3-Dimensional Brain Microvessels. *J Infect Dis* **230**, e1402–e1411 (2024).
725 85. Reyes, R. A. *et al.* Broadly inhibitory antibodies to severe malaria virulence proteins. *Nature*
726 **636**, 182–189 (2024).
727 86. Lipowsky, H. H. Microvascular Rheology and Hemodynamics. *Microcirculation* **12**, 5–15
728 (2005).
729 87. Hughes, C. S. *et al.* Ultrasensitive proteome analysis using paramagnetic bead technology.
730 *Molecular Systems Biology* **10**, 757 (2014).
731 88. Hughes, C. S. *et al.* Single-pot, solid-phase-enhanced sample preparation for proteomics
732 experiments. *Nat Protoc* **14**, 68–85 (2019).
733 89. Dayon, L. *et al.* Relative Quantification of Proteins in Human Cerebrospinal Fluids by MS/MS
734 Using 6-Plex Isobaric Tags. *Anal. Chem.* **80**, 2921–2931 (2008).
735 90. Kong, A. T., Leprevost, F. V., Avtonomov, D. M., Mellacheruvu, D. & Nesvizhskii, A. I.
736 MSFragger: ultrafast and comprehensive peptide identification in mass spectrometry–based
737 proteomics. *Nat Methods* **14**, 513–520 (2017).
738 91. Ritchie, M. E. *et al.* limma powers differential expression analyses for RNA-sequencing and
739 microarray studies. *Nucleic Acids Research* **43**, e47 (2015).
740 92. Huber, W., von Heydebreck, A., Sültmann, H., Poustka, A. & Vingron, M. Variance
741 stabilization applied to microarray data calibration and to the quantification of differential
742 expression. *Bioinformatics* **18 Suppl 1**, S96-104 (2002).

743

744